

3 RESULTS

Neuroblastoma (NB) is the most common extra cranial tumor of the childhood. Treatment for NB differs largely from patient to patient, depending upon the aggressiveness of the disease. NB is treated like non-small cell lung cancer (NSCLC) of adults. Chemotherapy drugs that are being used for treatment of NB have their own toxicity. As NB is a pediatric cancer, present treatment regimens that target the cell proliferation and regression of cancer cells, may have negative impact on normal growth of the child. Therefore, there is a need to focus on target specific phytochemical-based therapy which has promising activity as potential druggable molecule.

In proposed research work, IGF-IR specific inhibitor, Picropodophyllotoxin (PPP), was used to ablate IGF-IR, which governs the signal transduction in NB pathogenesis.

PPP interacts and binds with the ATP binding domain of the IGF-IR. PPP is an inhibitor of the IGF-IR, a surface receptor kinase which is over-expressed in many cancers. The overexpression of IGF-IR is observed in NB with its identified surface receptor marker, ALK. If a single therapeutic molecule is found which can bind and inhibit to both, IGF-IR and ALK, it can lead to development of better treatment options for NB. Molecular docking carried by AutoDock Vina reveals that the binding affinity of PPP with IGF-IR is -7.5 kcal/mol (Fig. 3.2) and with ALK is -8.8 kcal/mol (Fig 3.1). Results from molecular docking reveal that PPP not only binds and inhibits IGF-IR, but it has high binding affinity with the ALK.

The type of interactions that are formed between PPP and IGF-IR (Fig.-3.1) are conventional hydrogen bond, carbon-hydrogen bond, alkyl bond and pi-alkyl bond. The conventional hydrogen

bond is formed between the PPP and Gln1007 of the IGF-IR, which is at the 1007th position in chain 'A'. The length of this bond is 2.65 Å. The carbon-hydrogen interactions occur between the PPP and threonine, methionine and glycine of the IGF-IR, which are at the 1083rd, 1082nd and 1006th position respectively, in chain 'A'. The length of these bonds is 3.58 Å, 3.75 Å and 1.99 Å respectively. The alkyl interactions are occurring between the PPP and methionine, leucine, valine and alanine of the IGF-IR, which are at the 1142nd, 1005th, 1013th and 1031st position respectively, in chain 'A'. The length of these bonds is 5.19 Å, 4.4 Å, 5.36 Å and 3.92 Å respectively. The pi-alkyl interactions are occurring between the PPP and valine and leucine of IGF-IR, which are at the 1013th and 1031st position respectively, in chain 'A'. The length of these bonds is 5.18 Å and 5.37 Å, respectively.

The types of interactions that are formed between PPP and ALK (**Fig. 3.2**) are conventional hydrogen bond, carbon-hydrogen bond, alkyl bond, pi-alkyl bond, pi-pi stacked and pi-pi T shaped interactions. The conventional hydrogen bond is formed between the PPP and glycine of the ALK, which is at the 1123rd position in chain 'A'. The length of this bond is 2.85 Å. The carbon-hydrogen bonds are formed between the PPP and two glycine, arginine and histidine of the ALK, which are at the 1269th, 1202nd, 1253rd and 1124th position respectively in chain 'A'. The pi-pi stacked and pi-pi T shaped interactions are occurring between the PPP and phenylalanine of the ALK, which is at the 1127th position in chain 'A'. The alkyl and pi-alkyl interactions are occurring between the PPP and valine and two leucine amino acids of ALK, which are at the 1130th, 1122nd and 1256th position in chain 'A'.

For analysis of the cytotoxic effect of PPP, MTT assay was performed. To derive the IC₅₀ value of PPP, SH-SY5Y cells were treated with PPP for 24 hours with five different concentrations to derive the IC₅₀ value. The concentration of doses used were 0.89µM, 0.68µM, 0.48µM, 0.20µM

and 0.068 μ M. Percent inhibition of each dose was calculated and log dose graph was plotted against percent inhibition (Fig 3.3) using Origin 2021 version software. The IC₅₀ value of PPP derived on SH-SY5Y cells was 0.501 μ M. Formazan crystals are formed due to activity of mitochondrial enzymes. However, no crystals are formed when cells undergo apoptotic or necrotic pathways. So, to derive the dose for further work on cancer regression via ablation of IGF-IR, narrow range dose study was conducted. A dose which resulted in induction of programmed cell death via kinase inhibition but not in necrotic path was selected. The derived dose to study for further analysis of anti-cancer effect of PPP was 16nM, where zilch occurrence of necrotic phenomenon was observed.

NB cells were treated by PPP (16nM concentration) for 24 hours. Treated cells were used for total RNA, miRNA and protein isolation. Gene expression of *IGF1R* was validated by western blot that was further confirmed by immunocytochemical localization at cellular level. Change in the transcript level expression was calculated as fold change by $2^{-\Delta\Delta CT}$. Transcript expression of untreated cells of NB was considered as '1' fold. After 24 hours of PPP treatment transcript level of *IGF1R* was observed to be downregulated. The fold change of *IGF1R* expression was observed to be suppressed by 0.093 ± 0.002 fold (Fig. 3.4 D). This result was found to be statistically significant ($p \leq 0.0001$). Post translational level validation was performed by western blot. After the normalization of proteins with β -actin, expression level of IGF-IR (Fig. 3.4 A, C) and pIGF-IR (Fig. 3.4 B, C) was measured using ImageJ software. Protein expression of IGF-IR and pIGF-IR after 24 hours of PPP exposure was observed to be down regulated. The expression of IGF-IR was down regulated by 0.348 ± 0.003 ($p \leq 0.0001$). The protein expression of phosphorylated IGF-IR (pIGF-IR) was also observed to be low (0.0937 ± 0.005). The protein expression level found was significantly lower than that of the non-treated NB cells ($p \leq 0.0001$).

IGF-I ligand binds to IGF-I receptor (IGF-IR) as well as to insulin receptor (IR), thus activating many hallmark pathways of cancer. Along with IGF-IR, western blot of IR was also performed to validate the protein level expression of IR. On exposure of IGF-IR inhibitor to neuroblastoma cells, low level of IR expression was observed. Expression was down regulated by 0.964 ± 0.025 that was statistically non-significant (Fig. 3.5).

Amplification of anaplastic lymphoma kinase (ALK), a membrane-bound tyrosine kinase, is present in ~14 percent of newly diagnosed patients with high-risk NB. Docking result suggests that PPP is an ATP binding competitor, therefore, ALK expression was taken under consideration. Gene and protein level expression was measure after treatment of PPP. Transcript level expression of *ALK* was measured to be downregulated by 0.624 ± 0.034 fold which is statistically significant ($p \leq 0.01$) (Fig. 3.6 C). Western blot analysis reveals decreased protein expression of ALK in PPP treated NB cells by 0.70 ± 0.032 with significance of $p \leq 0.001$ (Fig 3.6 A,B).

Inhibition of IGF-IR, a receptor-tyrosine kinase, may lead to altered activity of downstream cascade proteins. For further analysis of PPP's inhibitory effect on NB cells via suppression of the IGF-IR, expression levels of *PI3K*, *AKT* and *CDK* were selected to investigate in the present proposal. Low level of transcript expression was found for *PI3K*, *AKT* and *CDK* on exposure of IGF-IR inhibitor. The expression was observed to be downregulated by 0.074 ± 0.0043 , 0.04 ± 0.0045 and 0.036 ± 0.0047 respectively (Fig. 3.7 A). The phosphorylation of kinases is one of the known neoplastic feature required to maintain the metastasis state of the tumor. On the suppression of transcript level expression of kinases, downstream molecular cascade involved in cancer progression was discontinued, which may result into cancer regression.

Hyperactivation of kinases and their transcriptional targets which act as mitogenic regulator is often associated with oncogenesis. Therefore, *MYCN* and *NFκB*, transcription factor was selected

for the study. On the basis of amplification of *MYCN*, NB cancer is categorised as *MYCN*⁺ or *MYCN*⁻. Occurrence of *MYCN* overexpression is common in NB tumour. After 24 hours of treatment of IGF-IR inhibitor, *MYCN* expression was found down regulated by 0.329 ± 0.01 ($p \leq 0.001$). p65 subunit of *NFκB* translocates into nucleus and regulates the expression of genes that regulate cell proliferative. Downregulation by 0.065 ± 0.021 fold was measured for *NFκB* gene after 24 hours of PPP treatment (Fig. 3.8 A). Result was further supported by ICC. It was postulated that on suppression of mitogenic gene in neoplastic state, expression of *p53*, a tumour suppressor gene, may increase. p53, a regulator of cell cycle, expresses at low level in cancer cell that allows cell to proliferate in an uncontrolled manner, making them immortal. In current study, when SH-SY5Y cells were treated by PPP, expression of *p53* was found high by 5.625 ± 0.16 fold. The value was found to be statistically significant ($p \leq 0.0001$).

Cell proliferation and metastasis state of tumor is associated with persistent EMT. If tumor cells transit from EMT to MET, it may lead to cancer cell death. Here, expression of E-cadherin, *SNAIL*, *TWIST*, *TUBULIN* and *NANOG* genes were investigated for EMT study (Fig. 3.8 B). E-cadherin is an epithelial marker and its low expression is observed in cancer cell which allows cell to proliferate. We had hypothesised that, if increase in E-cadherin expression is achieved by the treatment of PPP, it will lead to altered EMT and anoikis of the cancer cells. Upregulation of *E-cadherin* transcript was found higher by 19.58 ± 0.38 fold that is statistically significant ($p \leq 0.0001$) represents expression of mesenchymal marker (Fig. 3.8 B). Downregulation of transcript expression was observed for *SNAIL* (0.087 ± 0.003), *TWIST* (0.058 ± 0.003), *TUBULIN* (0.117 ± 0.02) and *NANOG* (0.041 ± 0.003) (Fig. 3.8 B). *NANOG* involves for stemness factors in cancer progression. NB is embryonic cancer, if stemness factors in somatic cells is able to reprogram the cells back to an embryonic stem cell-like state that stimulate NB tumour cells to differentiate. On differentiation, cancer undergoes regression.

If cancer cell loses its properties by down regulation of proliferation and EMT markers, it undergoes programmed cell death. BCL-2 and BAX, mitochondrial specific antiapoptotic and apoptotic marker respectively, were taken into consideration in study. Expression of *BCL2* was found downregulated (0.05123 ± 0.01) whereas *BAX* expression was found upregulated (9.244 ± 0.14) (Fig. 3.7A). Expressions were observed to be statistically significant ($p \leq 0.0001$). This result was supported by FACS and AO/EtBr staining.

Abnormal expression and regulation of miRNAs have been documented in various cancers. Establishing proper levels of miRNA expression can normalize the gene regulatory network and signaling pathways, which may aid in reversing the phenotype in cancerous cells.

miR-223 is a potential diagnostic and prognostic marker for many cancers. qRT-PCR analysis of the expression of miR-223 in NB cells was normalized to small RNA U6. Score of miR-223 was 88 with *IGF1R* and 89 with *CDK*. Upregulation of miR-223 was found by 4.642 ± 0.8135 fold which is statistically significant ($p \leq 0.05$) (Fig. 3.9). Upregulation of miR223 promotes inhibition of *IGF1R* and *CDK* translation via binding at 3' UTR.

miR-9 has been implicated in the enhancement of metastatic properties of cancer cells. Score of miR-9 was 84 with *CDK* and 88 with *PI3K*. Downregulation of miR-9 was found by 0.19 ± 0.06 fold which is statistically significant ($p \leq 0.001$) (Fig. 3.9).

Of all the tumor suppressor miRNAs, reduction in expression of let-7 occurs most frequently in the cancers. Score of let-7 was 98 with *PI3K* and 80 with *IGF1R*. Upregulation of this miRNA could lead to cancer regression as it suppresses various oncogenes. Upregulation of let-7 miRNA was found by 7.4 ± 1.682 fold which is statistically significant ($p \leq 0.05$) (Fig. 3.9).

For analyzing gene and protein level expression, molecules are extracted from total cells which essentially gives us a mean estimate of expression pattern in all of the cells. In immunocytochemistry, localization of protein expression at cellular level provides individual cell specific pattern. Therefore, it is a reflection of each cell's physiological reaction against the treatment molecule. For immunolocalization of IGF-IR, human anti-IGF-IR β primary antibody was used. Captured images were analyzed using ImageJ software. Analysis revealed that the measured gray-value (fluorescence intensity) of untreated cells was 24.31 ± 2.8 , whereas the gray-value intensity of PPP treated cells was low at 15.0 ± 1.2 (Fig. 3.10). The measured intensity was significantly low ($p \leq 0.05$) in treated cells in comparison to untreated cancerous cells.

Dissociation of NF- κ B heterodimer into p65 and p50, initiates the functional role of p65 as a transcription factor, regulator of cell proliferation and survival. p65 translocates in nucleus and leads to uncontrolled cell proliferation in cancerous cells. Localization of NF- κ B was carried out in the neuroblastoma cells. Translocation of p65 subunit of NF- κ B in NB cells was blocked on treatment of PPP for 24 hours (Fig. 3.12). Measured gray-value intensity was low (14.56 ± 0.76) in the nucleus of PPP-treated cells as compared to that of the untreated cells (45.64 ± 1.06). The value was observed to be statistically significant ($p \leq 0.0001$).

Docking result suggests that PPP is an ATP binding competitor. Moreover, one of the NB's characteristic features is overexpression of ALK. Though PPP is specific to IGF-IR, it may have altered the phosphorylation of ALK upon binding at ATP binding domain or on inhibition of IGF-IR. Cellular level change in expression of ALK was investigated by ICC. Florescent intensity in terms of gray-value in the NB cells treated by IGF-IR inhibitor was measured using ImageJ software (Fig. 3.11). The data indicates that on exposure of PPP to SH-SY5Y cells, cellular

localization of ALK was down regulated (18.7 ± 3.08) when fluorescent intensity was compared with untreated cells (38.34 ± 1.9).

Fig. 3.13 indicates that PPP treated cells inhibits proliferation of NB cells. After 24 hours of incubation of SH-SY5Y cells with PPP, rate of cell proliferation was observed low which resulted in a distinct gap with formed scratch. The observed scratch closure of SH-SY5Y cells in control condition was 1.45 mm, whereas the closure was 1.88 mm in PPP treated SH-SY5Y cells. Data suggests that on exposure of IGF-IR inhibitor, cells lose its characteristic feature of uncontrolled proliferation, that resulted in an uncovered wound that was formed using a pipette tip.

When IGF-IR signalling is altered, as well as when the cancer cells loses its power of uncontrolled proliferation and gets arrested in the cell cycle, it undergoes apoptosis. On exposure of IGF-IR specific inhibitor, induction of programmed cell death was measured using fluorescent assorted cell cytometry. Cells were stained by Annexin V/PI after treatment and cell death was analysed using FACS. H_2O_2 treated cells were used as positive control. In comparison to NB cells, percent of apoptotic cells (12.48%) was observed higher in cells treated by PPP (49.17%). Data suggest that cells underwent apoptotic cell death upon exposure of IGF-IR inhibitor (Fig. 3.14).

Morphological feature of SH-SY5Y was observed by AO/EtBr staining for confirmation of PPP induced apoptotic cell death after 24 hours of treatment. Nuclear condensation and cell shrinkage are the characteristic features of apoptotic cells that was observed due to PPP treatment (Fig. 3.15). Acridine orange stains viable cells which gives green fluorescence, but with early apoptotic cells it gives yellow fluorescence whereas with late apoptotic cells along with ethidium bromide its gives orange fluorescence. EtBr is only taken up by necrotic cells and it gives red fluorescence.

Based on these features, it was observed that a greater number of cells were in the apoptotic phase on treatment of IGF-IR inhibitor (Fig. 3.15).

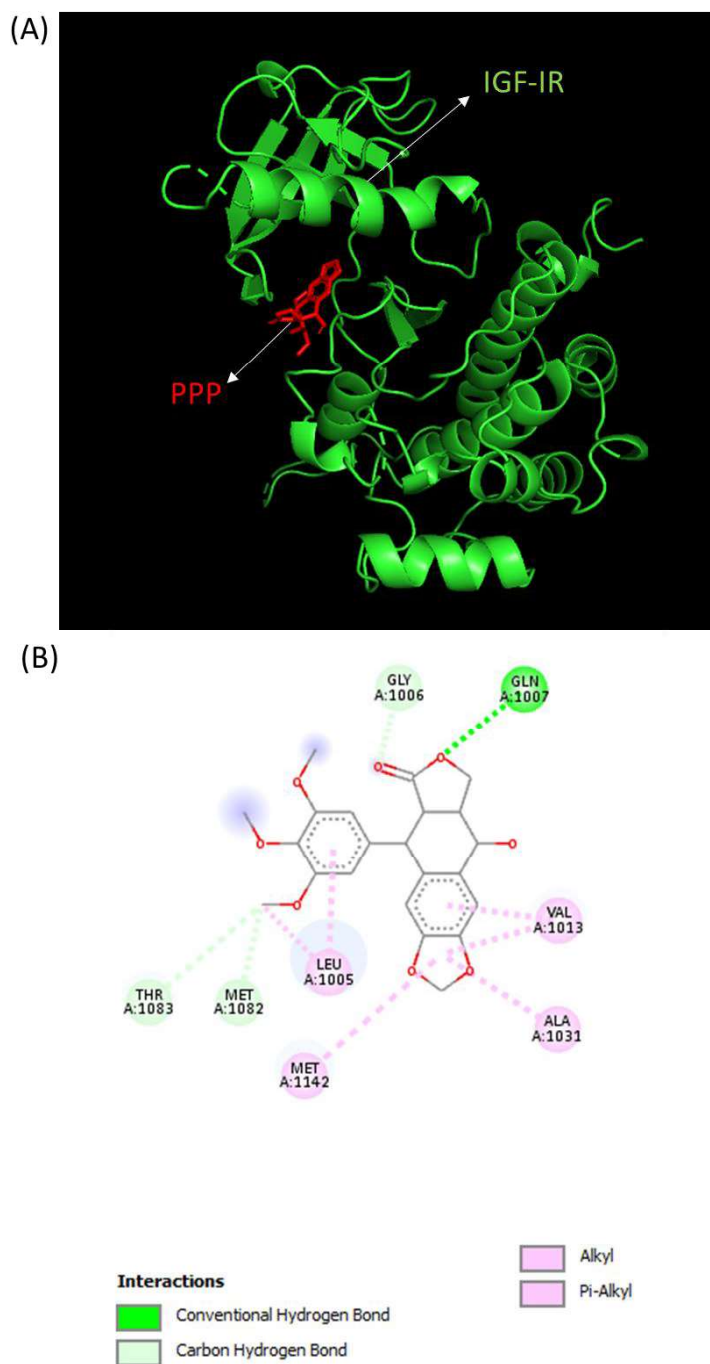


Fig 3.1: Molecular docking of ligand-protein. Docking of PPP with IGF-IR (PDB Id: 5fxq). A) 3D representation of docking. B) 2D representation of docking showing amino acid interactions with the PPP ligand atoms.

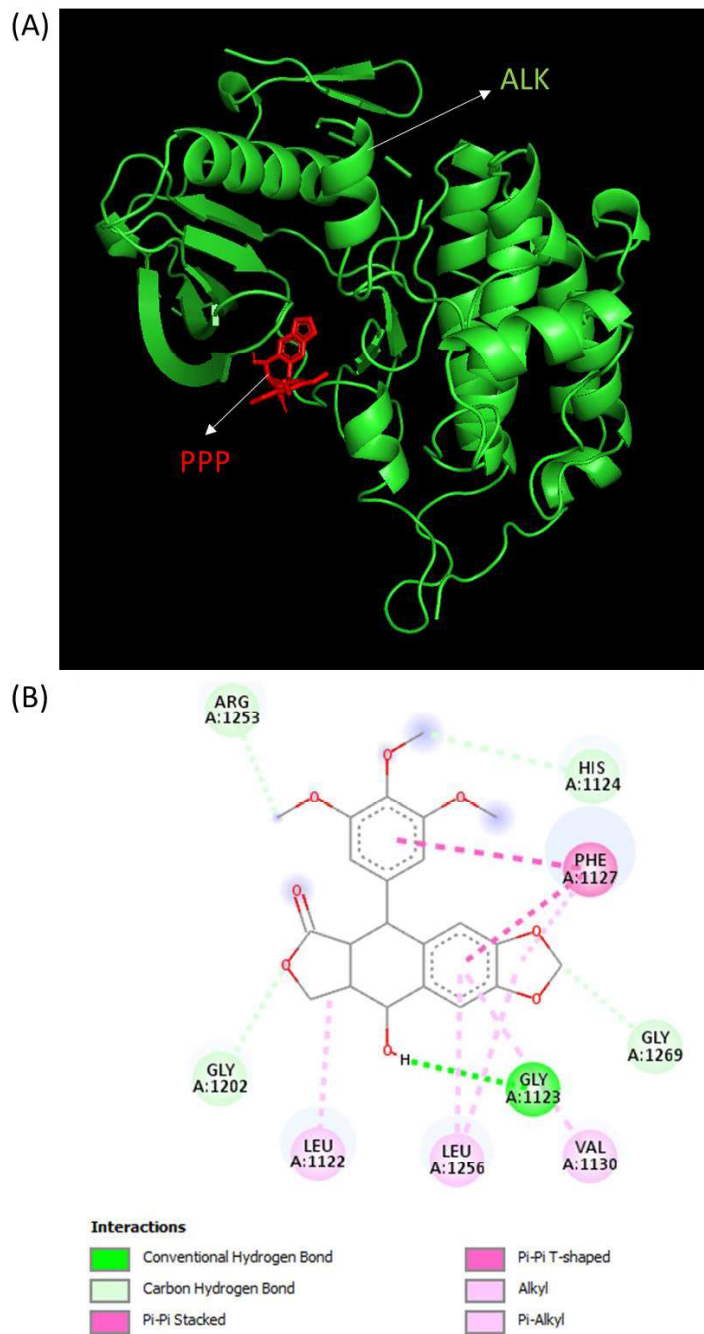


Fig 3.2: Molecular docking of ligand-protein. Docking of PPP with ALK (PDB Id: 5fto). A) 3D representation of docking. B) 2D representation of docking showing amino acid interactions with the PPP ligand atoms.

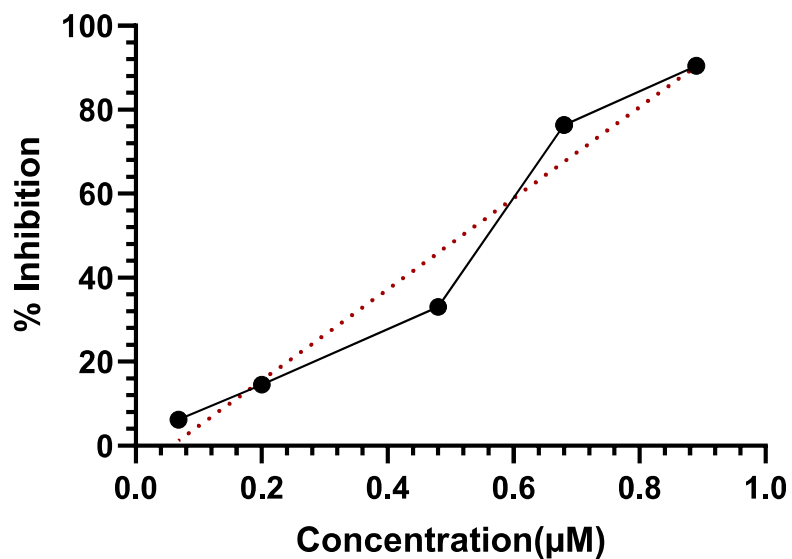


Fig 3.3: Effect of PPP on proliferation of NB cells after 24 hours of incubation. SH-SY5Y cells were treated with PPP in five different concentrations (0.89, 0.68, 0.48, 0.2 and 0.068 µM), growth inhibition of cells was detected by MTT assay. Graph was prepared using Origin 2021 version software.

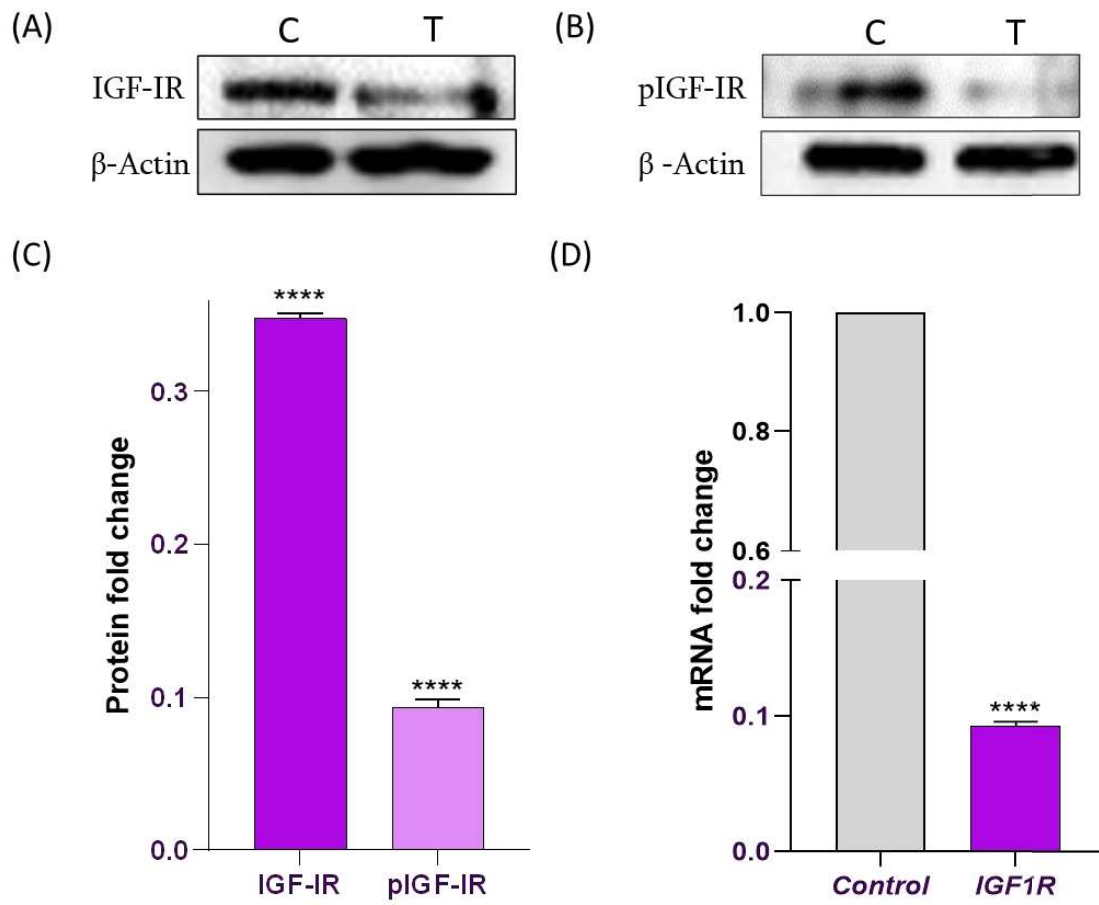


Fig 3.4: Gene and protein expression fold change of IGF-IR after 24 hours of PPP treatment to SH-SY5Y cell line. Western blot results were measured by densitometric analysis. Level of IGF-IR and pIGF-IR were normalized to β -actin. Fold change in gene expression was analysed using qPCR. Gene expression of *IGF1R* was normalized to GAPDH. Statistical analyses were performed on data. Values represents the Mean \pm SEM. (**** = $p \leq 0.0001$). A) Western blot result of IGF-IR, B) Western blot result of pIGF-IR, C) Protein fold change of IGF-IR and pIGF-IR, D) Fold change in gene expression of *IGF1R* in comparison to untreated NB cells.

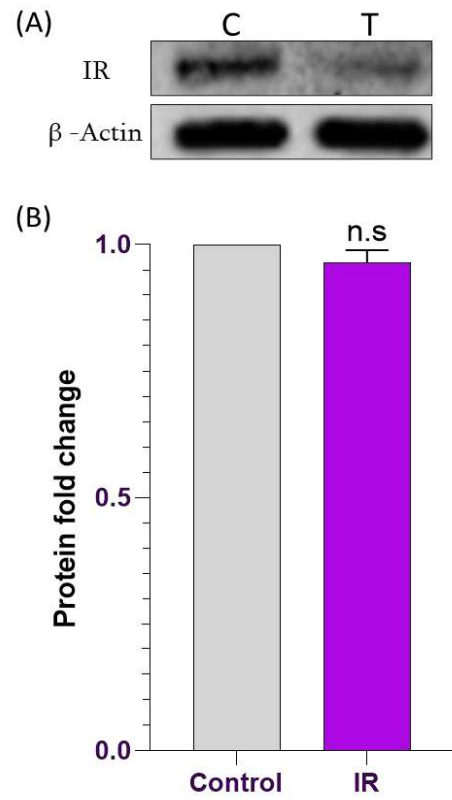


Fig 3.5: Protein expression fold change of IR after 24 hours of PPP treatment to SH-SY5Y cell line. Western blot results were measured by densitometric analysis. Level of IR was normalized to β actin. Statistical analyses were performed on data. Values represents the Mean \pm SEM. (n.s = not significant). A) Western blot result of IR, B) Protein fold change of IR.

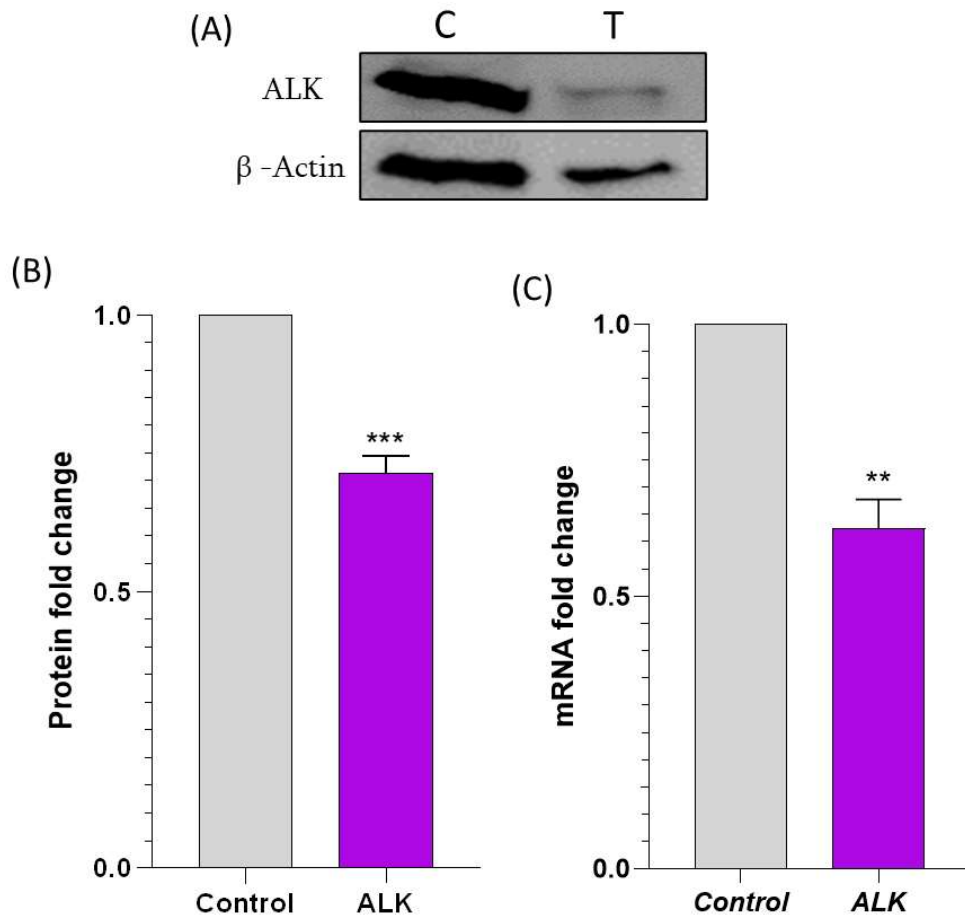


Fig 3.6: Gene and protein expression fold change of ALK after 24 hours of PPP treatment to SH-SY5Y cell line. Western blot results were measured by densitometric analysis. Level of ALK was normalized with β -actin. Fold change in gene expression was analysed using qPCR. Gene expression of *ALK* was normalized to GAPDH. Statistical analyses were performed on data. Values represents the Mean \pm SEM. (** = $p \leq 0.01$; *** = $p \leq 0.001$). A) Western blot result of ALK, B) Protein fold change of ALK, C) Fold change in gene expression of *ALK* in comparison to untreated NB cells.

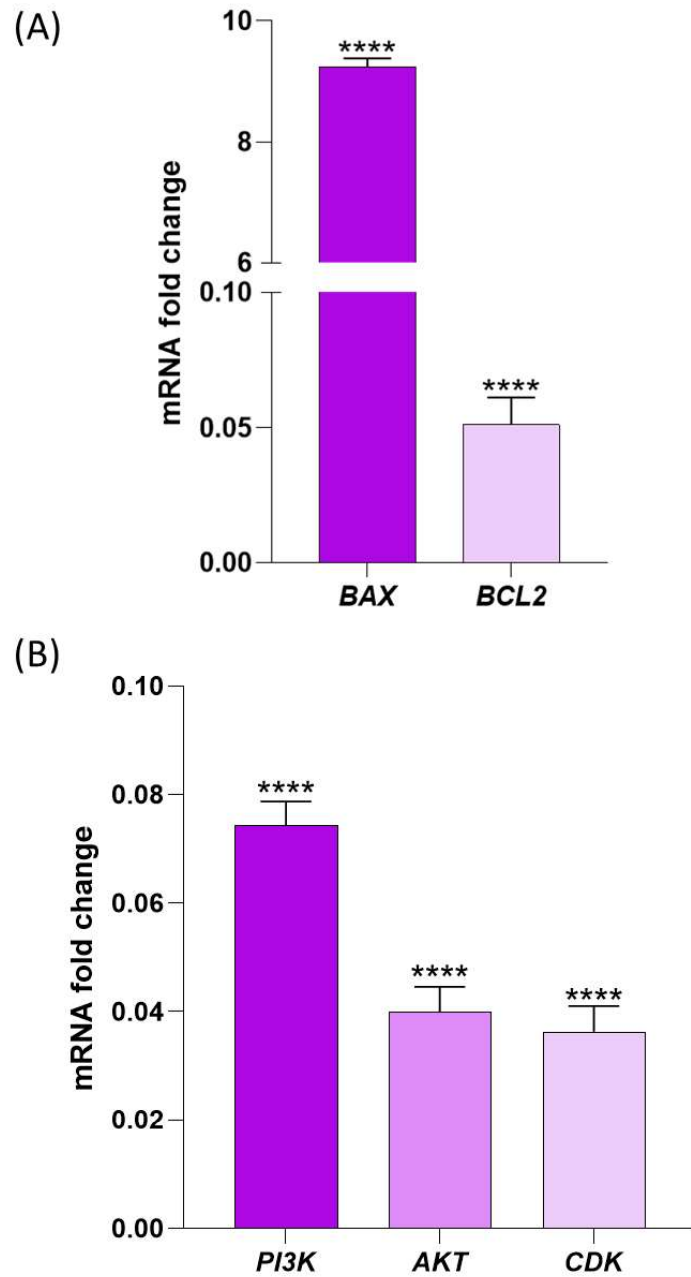


Fig 3.7: Transcript expression representation as fold change after 24 hours of PPP treatment to SH-SY5Y cell line. Fold change in gene expression was analyzed using qPCR. Expression of mRNAs were normalized with *GAPDH*. Statistical analyses were performed on data. Values represents the Mean±SEM. (****= $p \leq 0.0001$). A) Fold change in gene expression of *BAX* and *BCL2* apoptotic markers, B) Fold change in gene expression of *PI3K*, *AKT* and *CDK kinases*.

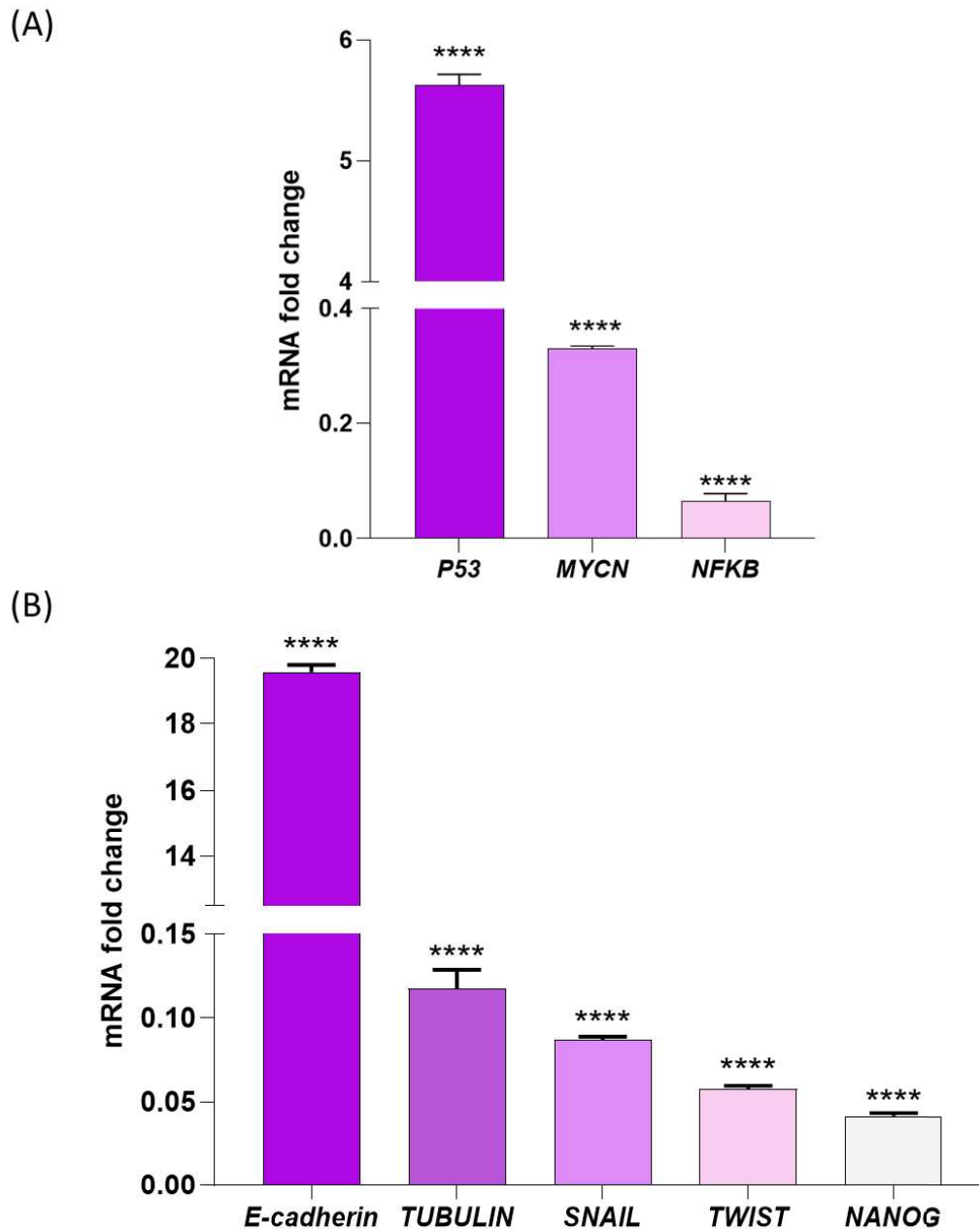


Fig 3.8: Gene expression fold change after 24 hours of PPP treatment to SH-SY5Y cell line. Fold change in gene expression was analysed using qPCR. Expression of mRNAs were normalized to GAPDH. Statistical analyses were performed on data. Values represents the Mean±SEM. (****= $p \leq 0.0001$). A) Fold change in gene expression of *p53*, *MYCN* and *NFKB* transcription factors, B) Fold change in gene expression of *E-cadherin*, *TUBULIN*, *SNAIL*, *TWIST* and *NANOG* EMT markers.

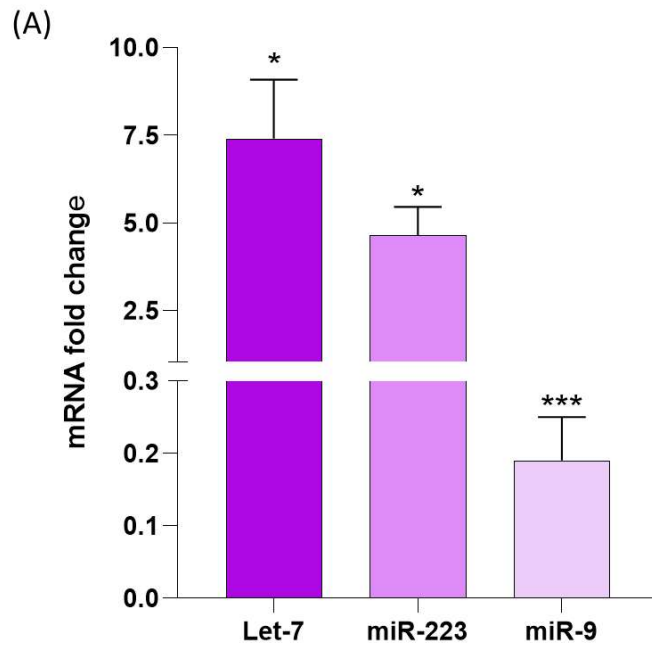


Fig 3.9: Representation of fold change in miRNA expression after 24-hour treatment of PPP. The expression of miRNAs was normalized to U6. Statistical analyses were performed on data. Values represents the Mean \pm SEM. (*= $p \leq 0.05$; ***= $p \leq 0.001$). The expression of miR-9 was observed downregulated, whereas expression of let-7 and miR-223 were upregulated.

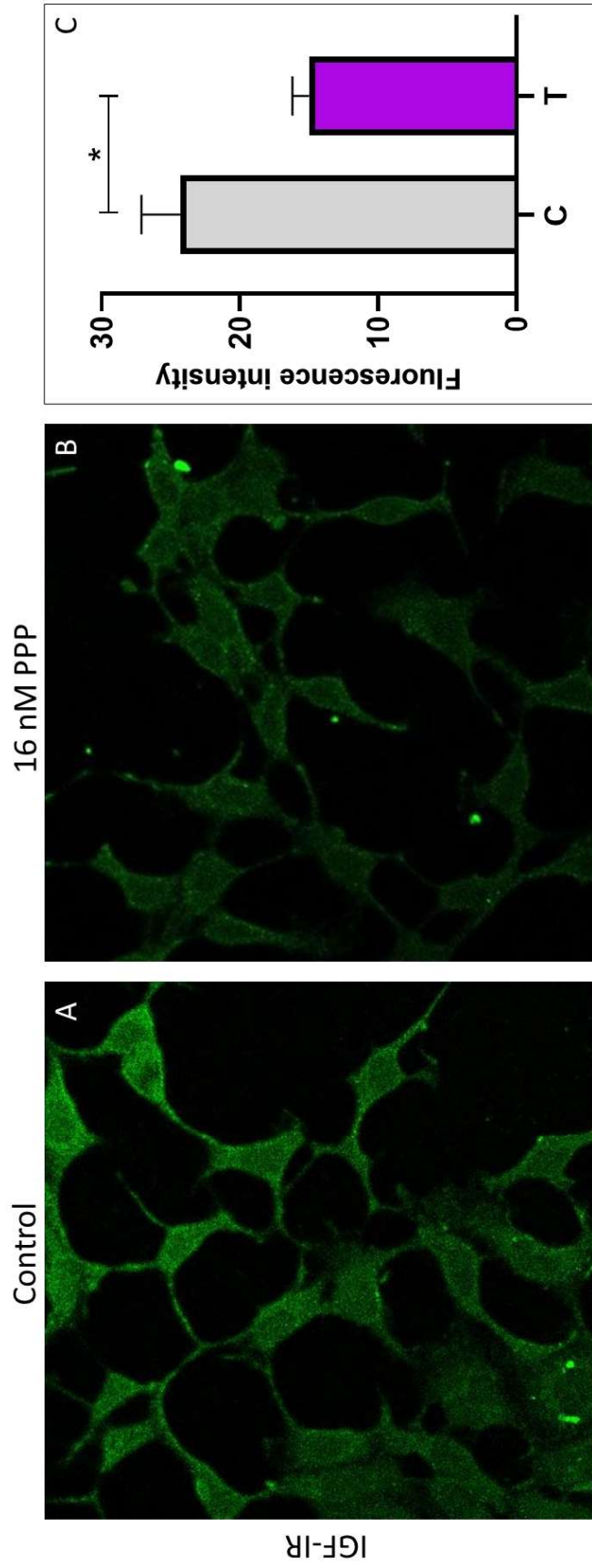


Fig 3.10: PPP treatment reduces expression of IGF-IR in NB cells. Expression of IGF-IR in Control (A) and Treated (B) cells, as visualised by ICC. (C) Fluorescence intensity of IGF-IR as measured by ImageJ software. All data is expressed as Mean \pm SEM. (63X magnification).

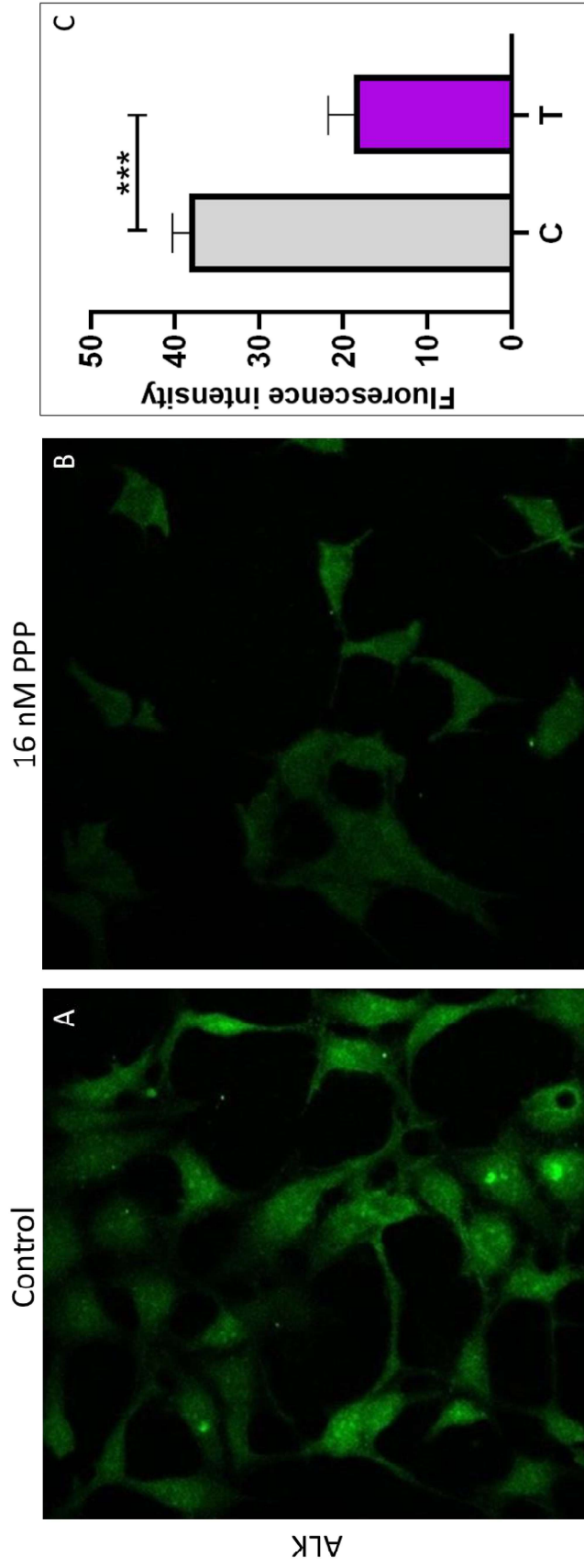


Fig 3.11: PPP treatment reduces expression of ALK in NB cells. Expression of ALK in Control (A) and Treated (B) cells, as visualised by ICC. (C) Fluorescence intensity of ALK as measured by ImageJ software. All data is expressed as Mean \pm SEM. (63X magnification).

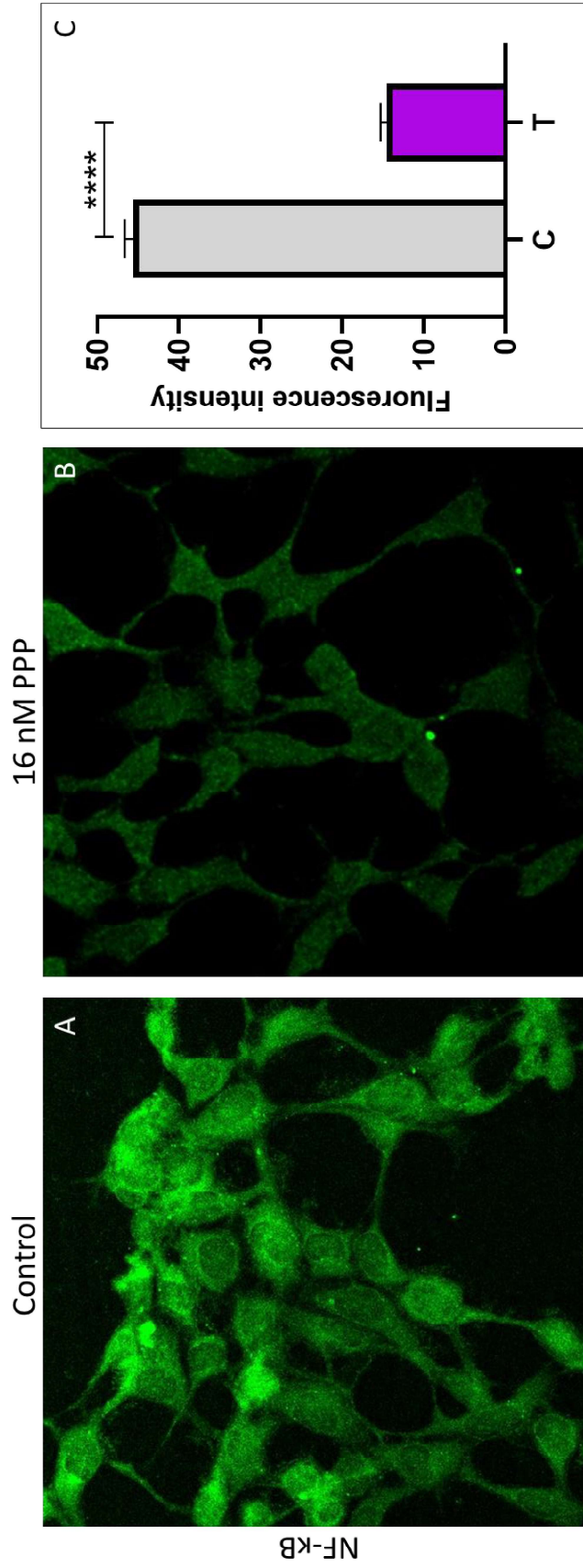


Fig 3.12: PPP treatment reduces expression of NF-κB in NB cells. Expression of NF-κB in Control (A) and Treated (B) cells, as visualised by ICC. (C) Fluorescence intensity of NF-κB as measured by ImageJ software. All data is expressed as Mean ± SEM. (63X magnification).

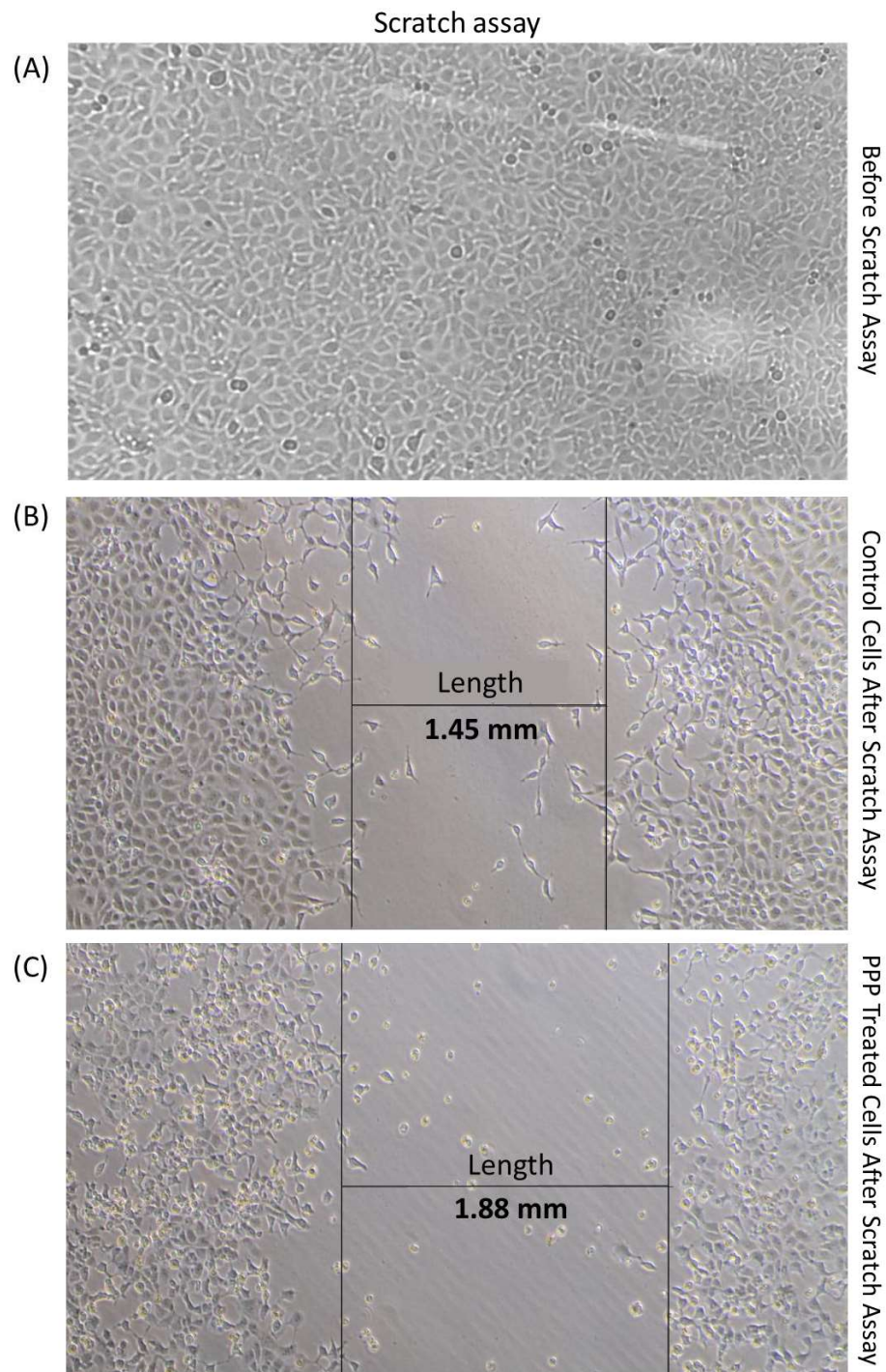


Fig 3.13: Representation of inhibition of cell proliferation using scratch assay. Cell proliferation is qualitatively assessed by visual inspection and quantitatively by measuring gap width. A) Confluent monolayer of cells before beginning scratch assay, B) At 24 hours post scratching, cells without treatment have started migrating and covering the wound. Width of the remaining scratch is 1.45 mm, C) At 24 hours post scratching, PPP treated cells still haven't started migrating. Width of the remaining scratch is 1.88 mm.

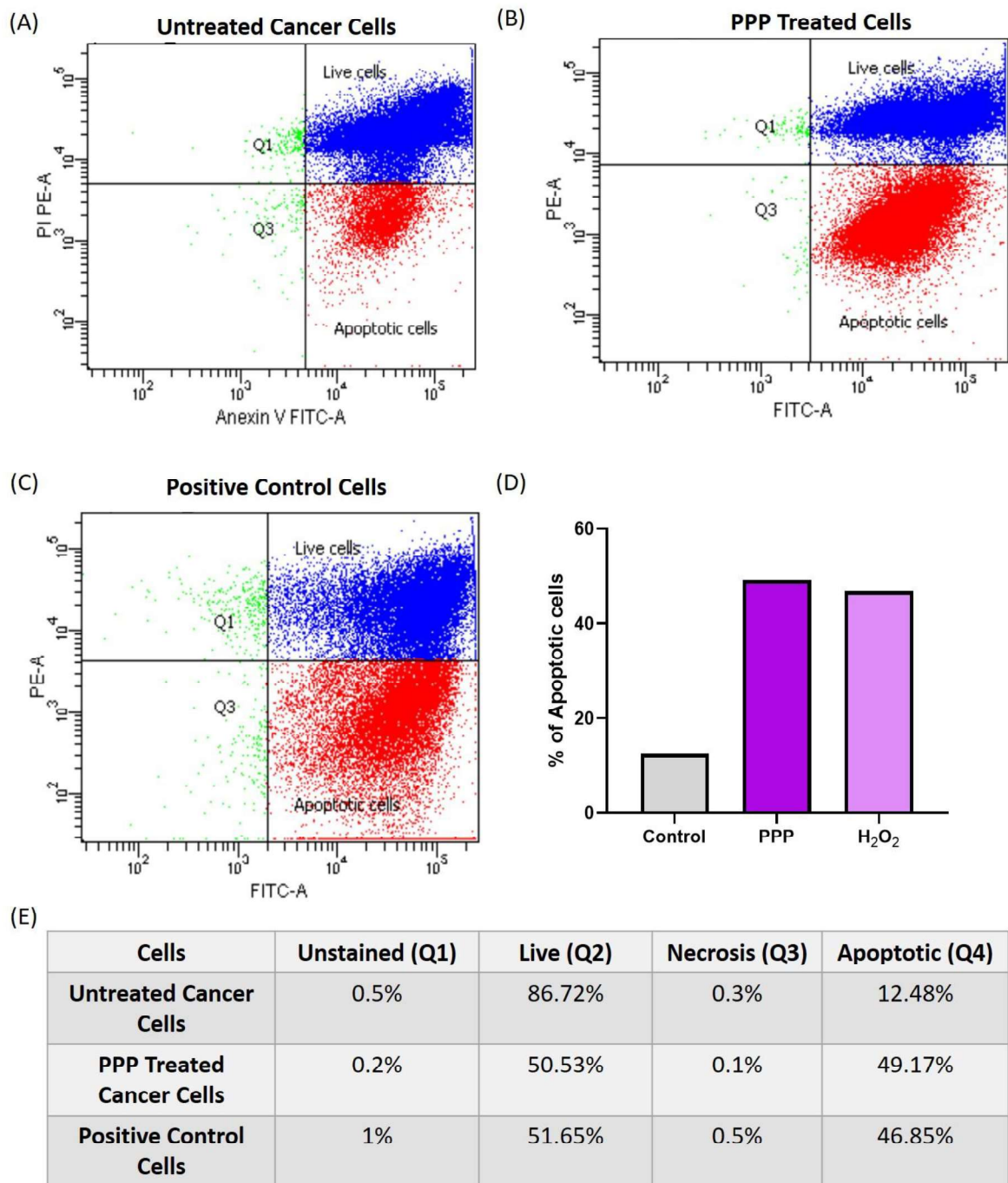


Fig 3.14: Annexin V-FITC/PI analysis using Flow cytometry for apoptosis inducing activities of Picropodophyllotoxin in SH-SY5Y cancer cells. Cells were treated by 16nm concentration of PPP for 24 hours. For positive control H_2O_2 was used. A). Untreated cells, B) Treated cells, C) Positive control cell, D) Graph for percent apoptotic cells, E) Table showing percent cells of each event of quadrant.

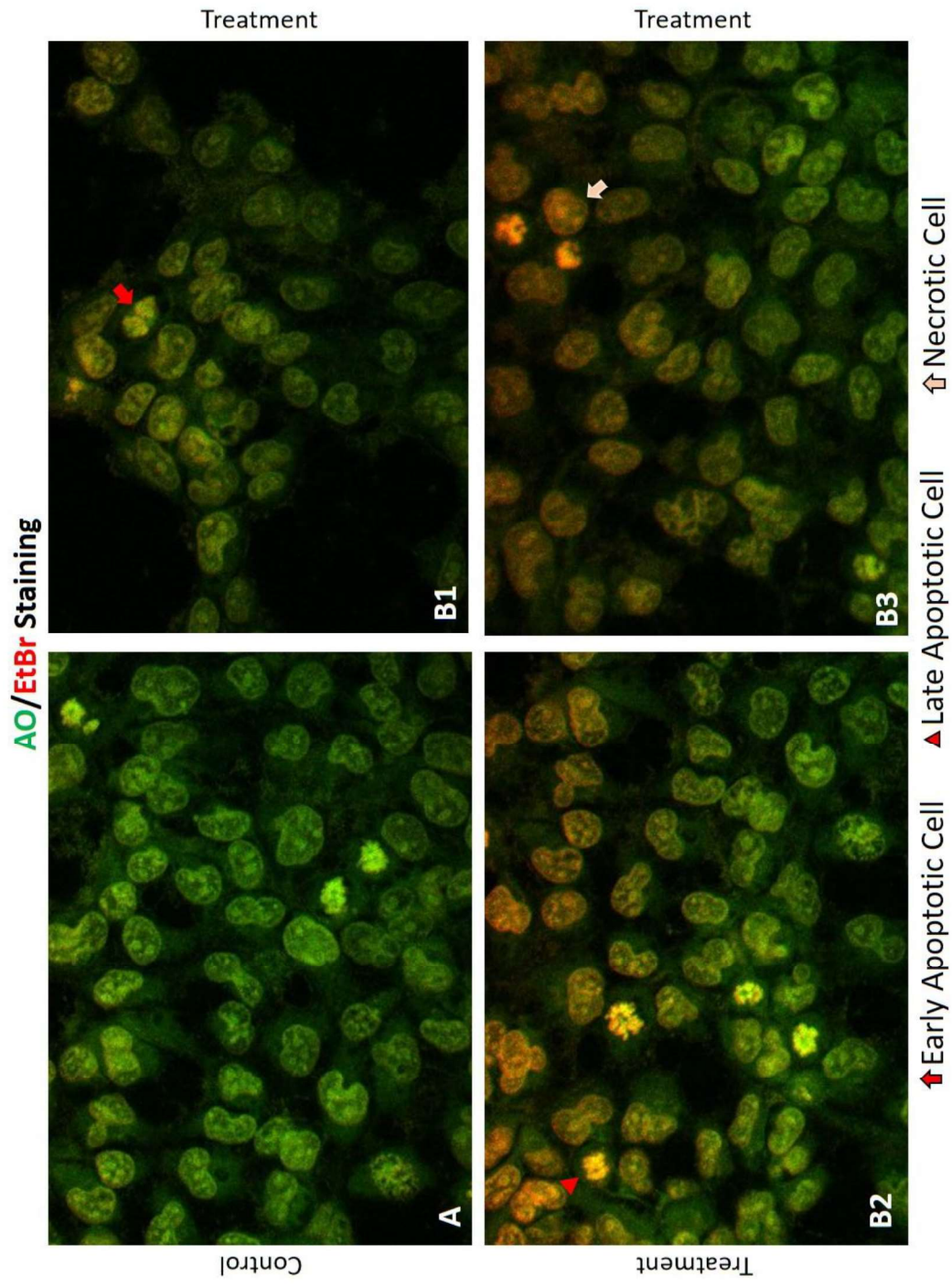


Fig. 3.15: Cell death analysis after 24 hours of PPP treatment to NB cells. Cells were stained by AO/EtBr. A) Control cells, B) Treated cells.

Table 3.1: Data values for fold change mRNA expression (n=3).

Gene	Mean	SEM	p value
<i>IGF1R</i>	0.093	0.003	≤ 0.0001
<i>AKT</i>	0.04	0.004583	≤ 0.0001
<i>PI3K</i>	0.07433	0.004372	≤ 0.0001
<i>CDK</i>	0.036333	0.004702	≤ 0.0001
<i>NFKB</i>	0.06523	0.021753	≤ 0.0001
<i>MYCN</i>	0.329	0.010	≤ 0.0001
<i>P53</i>	5.62532	0.15611	≤ 0.0001
<i>E-Cadherin</i>	19.58	0.38	≤ 0.0001
<i>TUBULIN</i>	0.11743	0.01958	≤ 0.0001
<i>SNAIL</i>	0.08718	0.00277	≤ 0.0001
<i>TWIST</i>	0.05765	0.00330	≤ 0.0001
<i>NANOG</i>	0.04133	0.00318	≤ 0.0001
<i>BAX</i>	9.3794	0.1359	≤ 0.0001
<i>BCL2</i>	0.05123	0.0100	≤ 0.0001

Table 3.2: Data values for fold change miRNA expression (n=3).

microRNA	Mean	SEM	p value
<i>miR-223</i>	4.642	0.813544	≤ 0.05
<i>Let-7</i>	7.4	1.682214	≤ 0.05
<i>miR-9</i>	0.19	0.060026	≤ 0.001

Table 3.3: Data values for fold change protein expression (n=3).

Protein	Mean	SEM	p value
IGF-IR	0.348	0.003	≤ 0.0001
pIGF-IR	0.0937	0.005	≤ 0.0001
IR	0.964	0.025	n.s
ALK	0.70	0.032	≤ 0.001